Received: 5 August 2019 | Revised: 23 January 2020 | Accepted: 2 March 2020

DOI: 10.1002/jbm.b.34607

ORIGINAL RESEARCH REPORT

Society For Biomaterials | WILEY

Comparison of two pore sizes of LAE442 scaffolds and their effect on degradation and osseointegration behavior in the rabbit model

Julia Augustin[1] | Franziska Feichtner[1] | Anja-Christina Waselau[1] | Stefan Julmi[2] | Christian Klose[2] | Peter Wriggers[3] | Hans Jürgen Maier[2] | Andrea Meyer-Lindenberg[1]

[1]Clinic for Small Animal Surgery and Reproduction, Ludwig-Maximilians-Universität, Munich, Germany

[2]Institut für Werkstoffkunde, Leibniz Universität Hannover, An der Universität 2, Garbsen, Germany

[3]Institute of Continuum Mechanics, Leibniz Universität Hannover, Hannover, Germany

Correspondence
Andrea Meyer-Lindenberg, Clinic for Small Animal Surgery and Reproduction, Ludwig-Maximilians-Universität, Munich, Germany.
Email: ameylin@lmu.de

Funding information
Deutsche Forschungsgemeinschaft, Grant/Award Number: 271761343

Abstract

The magnesium alloy LAE442 emerged as a possible bioresorbable bone substitute over a decade ago. In the present study, using the investment casting process, scaffolds of the Magnesium (Mg) alloy LAE442 with two different and defined pore sizes, which had on average a diameter of 400 μm (p400) and 500 μm (p500), were investigated to evaluate degradation and osseointegration in comparison to a ß-TCP control group. Open-pored scaffolds were implanted in both greater trochanter of rabbits. Ten scaffolds per time group (6, 12, 24, and 36 weeks) and type were analyzed by clinical, radiographic and μ-CT examinations (2D and 3D). None of the scaffolds caused adverse reactions. LAE442 p400 and p500 developed moderate gas accumulation due to the Mg associated in vivo corrosion, which decreased from week 20 for both pore sizes. After 36 weeks, p400 and p500 showed volume decreases of 15.9 and 11.1%, respectively, with homogeneous degradation, whereas ß-TCP lost 74.6% of its initial volume. Compared to p400, osseointegration for p500 was significantly better at week 2 postsurgery due to more frequent bone-scaffold contacts, higher number of trabeculae and higher bone volume in the surrounding area. No further significant differences between the two pore sizes became apparent. However, p500 was close to the values of ß-TCP in terms of bone volume and trabecular number in the scaffold environment, suggesting better osseointegration for the larger pore size.

KEYWORDS

biodegradation, magnesium, osseointegration, porous, scaffolds

1 | INTRODUCTION

The gold standard for larger bone defects is the use of autologous bone grafts with the advantage of osteoinductive, osteoconductive, and adapted mechanical properties (Yoshikawa & Myoui, 2005). However, the associated risk factors are numerous (Prolo & Rodrigo, 1985). Creating a second surgical site, limited availability and donor-site morbidity represent an additional burden for the patient and limit the applicability of bone grafts (Arrington, Smith, Chambers, Bucknell, & Davino, 1996; Banwart, Asher, & Hassanein, 1995; Younger & Chapman, 1989).

Commonly used alternatives are bone substitutes made of biocompatible, biodegradable ceramics (Nuss & von Rechenberg, 2008)

or polymers (Agarwal, Curtin, Duffy, & Jaiswal, 2016). However, ceramics such as ß-tricalcium phosphate (ß-TCP) are brittle and are susceptible to fatigue fractures, which limits their use under load (Ignatius et al., 2001). Studies have shown that the use of polymers such as polyglycolides (PGA) and polylactides (PLA) can trigger foreign body reactions while degrading (Bergsma, Rozema, Bos, & Bruijn, 1993; Böstman et al., 1989; Suganuma & Alexander, 1993). Due to a lack of long-term stability, their use is also restricted to areas of the bone that are not exposed to great stress (Agarwal et al., 2016).

In order to avoid or significantly reduce limited mechanical stability and biocompatibility, more attention is being paid to bioresorbable bone substitutes consisting of magnesium alloys (Agarwal et al., 2016). The mechanical properties such as the Young's modulus (E = 41–45 GPa) and the density (1.74–1.84 g/cm^3) of magnesium (Mg) are similar to bone (E = 15–25 GPa/density = 1.8–2.1 g/cm^3) (Staiger, Pietak, Huadmai, & Dias, 2006), so the use of Mg as a bioresorbable metal can ensure long-term stability during the healing phase (Angrisani, Seitz, Meyer-Lindenberg, & Reifenrath, 2012). At the beginning of the last century, investigations with Mg implants were already being carried out on humans and animals to analyse the degradation of pure Mg in the form of plates, screws, and pins (Lambotte, 1932; Mcbride, 1938; Verbrugge, 1933; Verbrugge, 1934). Due to too rapid degradation of implants made of pure Mg and the resulting gas formation ($Mg + 2H_2O \rightarrow Mg(OH)_2 + H_2$) these implants have not yet found broad clinical application (Song & Atrens, 1999; Staiger et al., 2006).

Recently, Mg was reintroduced as an implant material. The corrosion behavior of Mg could be slowed down by adding various elements such as aluminum (Al), zinc (Zn), lithium (Li), and rare earth elements (SE). This resulted in better primary stability with good biocompatibility (Angrisani et al., 2012; Angrisani et al., 2016; Hampp et al., 2013; Höh et al., 2009; Lalk et al., 2013; Lalk, Reifenrath, Rittershaus, Bormann, & Meyer-Lindenberg, 2010; Meyer-Lindenberg et al., 2010; Rossig et al., 2015; Thomann et al., 2009; Witte et al., 2005; Witte et al., 2006; Witte et al., 2010). Compared with Al-Zn alloys (AZ91, AZ31) and an alloy with yttrium and rare earths (WE43) (Witte et al., 2005), the Mg alloy LAE442 (90 wt% Mg, 4 wt% Li, 4 wt % Al, 2 wt%) has proven to be a promising implant in various animal studies with regard to its good mechanical stability and biocompatibility (Angrisani et al., 2012; Angrisani et al., 2016; Hampp et al., 2013; Meyer-Lindenberg et al., 2010; Reifenrath et al., 2010; Rossig et al., 2015; Witte et al., 2005; Witte et al., 2006; Witte et al., 2010).

The ideal bone substitute material should not only retain its mechanical stability, but also degrade over time in a controlled manner as new bone grows into the substitute (Phemister, 1935). Pores were incorporated into biodegradable bone substitutes in order to adapt to the structure of bone and promote the ingrowth of blood vessels and migration of bone progenitor cells (Kuboki et al., 1998). The size spectrum of the pores ranged from micropores (<100 μm) to macropores (up to about 1000 μm) and different porosities of the material were employed. Pore sizes in a range of 100–500 μm for ceramics as well as for metals proved to be beneficial for osseointegration (Bobyn, Pilliar, Cameron, & Weatherly, 1980; Bohner et al., 2017; Cheng et al., 2016; Galois & Mainard, 2004; Hofmann et al., 2013; Hulbert et al., 1970; Itälä, Ylänen, Ekholm, Karlsson, & Aro, 2001; Karageorgiou & Kaplan, 2005; Klenke et al., 2008; von Doernberg et al., 2006).

In a preliminary study, the MgF_2 coated alloy AX30 used as a porous sponge with inhomogeneously distributed pores showed good osseointegration in a rabbit model, but its degradation was still too fast (Lalk et al., 2013). The objective of the present study was to investigate the slow degrading LAE442 alloy for the first time as reproducible, porous scaffolds, instead of solid bodies used as bone substitute material in former investigations (Angrisani et al., 2016; Hampp et al., 2013; Meyer-Lindenberg et al., 2010; Reifenrath et al., 2010; Rossig et al., 2015; Witte et al., 2005; Witte et al., 2006). Since pore sizes of a bone substitute also play an important role in the formation of new bone tissue (Karageorgiou & Kaplan, 2005), the osteoconductive properties of two different pore sizes of LAE442 were also compared in the present study.

2 | MATERIALS AND METHODS

2.1 | Magnesium alloy and scaffold structure

The magnesium alloy LAE442 (4 wt% lithium, 4 wt% aluminum, 2 wt% rare earths) was produced using the manufacturing process suggested by Seitz et al. (2011).

To produce the porous scaffolds, exact models of the scaffolds were created using the fused deposition modeling process with individual successive layers of wax on a 3D printer (Solidscape, Inc., Merrimack) (Julmi, Klose, Krüger, Wriggers, & Maier, 2017). For the following investment casting process, the resulting single wax cylinders were attached together to a model wax tree. A subsequent dipping process of this wax tree in gypsum (Gilcast AM, BK Giulini GmbH, Ludwigshafen, Germany) produced the final casting mold for the scaffolds. The subsequent firing process hardened the casting mold and melted out the pattern material. Two versions of the cylindrical LAE442 scaffolds (Ø 4 mm, height 5 mm, n = 40 per version) were manufactured. Both scaffold models had homogeneously arranged interconnecting pores. The first model featured an average pore size of 400 μm (p400) with intermediate strut elements of 0.4 and 0.3 mm, a porosity of 43% and a volume of 37 mm^3. The second model had an average pore size of 500 μm (p500), strut elements of 0.4 and 0.5 mm, a porosity of 41% and a volume of 38 mm^3 (Figure 1). The cast scaffolds were coated with a MgF_2 layer using the "conversion coating method" (Julmi et al., 2019).

The control group consisted of commercially available resorbable ß-TCP (Cerasorb M, Curasan AG, Kleinostheim, Germany), which was produced in corresponding dimensions (Ø 4 mm, height 5 mm) for this study with a porosity of 65% (micro-, meso- and macropores ≤500 μm). Prior to implantation, the scaffolds were sterilized by gamma rays of >29 Gry (BBF-Sterilisations service GmbH, Kernen, Germany).

2.2 | Animal model

The animal experiments were approved with the reference number ROB 55.2-1-54-2532-181-2015 by the regional government of Upper Bavaria, under paragraph 8 of the Animal Welfare Act. Sixty adult female ZIKA rabbits (Assamhof, Kissing, Germany) with an average weight of 3.93 kg (± 0.27 kg) were used for this study. The animals were randomly divided into scaffold and time groups. According to the study by Lalk et al. (2010), two scaffolds (one per hind limb) were implanted per rabbit in the cancellous part of the greater trochanter of the femur (Figure 2a). In all three groups (p400, p500, and ß-TCP) a total of 40 scaffolds were used. These remained for investigation periods of 6, 12, 24, and 36 weeks respectively, so that a total of 10 scaffolds per time group were examined. The animals were kept in accordance with the European Convention for the protection of vertebrate animals used for experimental and other scientific purposes (Appendix A, ETS 123). In addition to rationed commercial pellet feed (Kanin Kombi, Rieder Asamhof GmbH & Co KG, Kissing, Germany), hay and water were provided ad libitum.

2.3 | Operation

Anaesthesia was induced intramuscularly with 0.15 mg/kg ketamine (Anesketin® 100 mg/ml, Albrecht GmbH, Aulendorf, Germany) and 0.25 mg/kg medetomidine (Dorbene vet® 1 mg/ml, Zoetis Deutschland GmbH, Berlin, Germany). A venous catheter was placed in the auricular vein of the animals. The animals were intubated and the

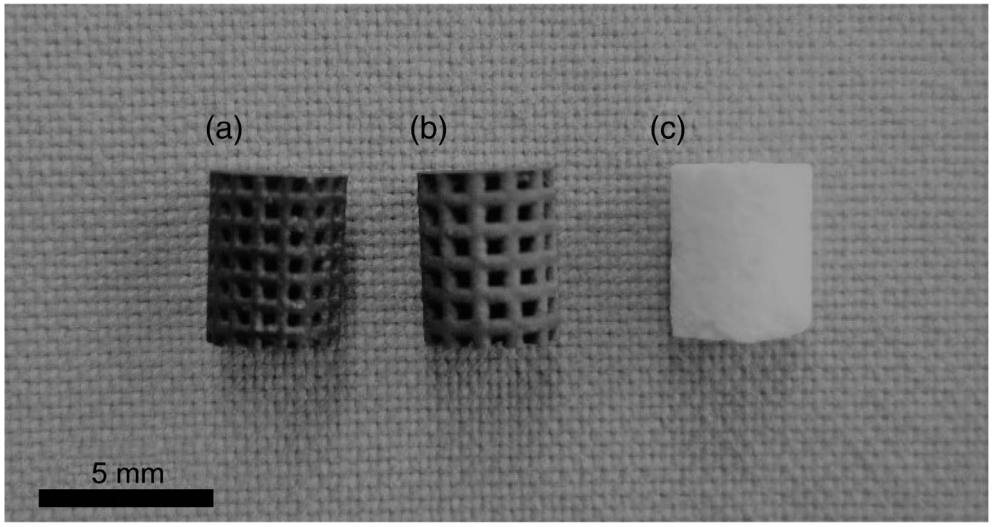

FIGURE 1 Scaffold types used (a) LAE442 p400, (b) LAE442 p500, (c) ß-TCP

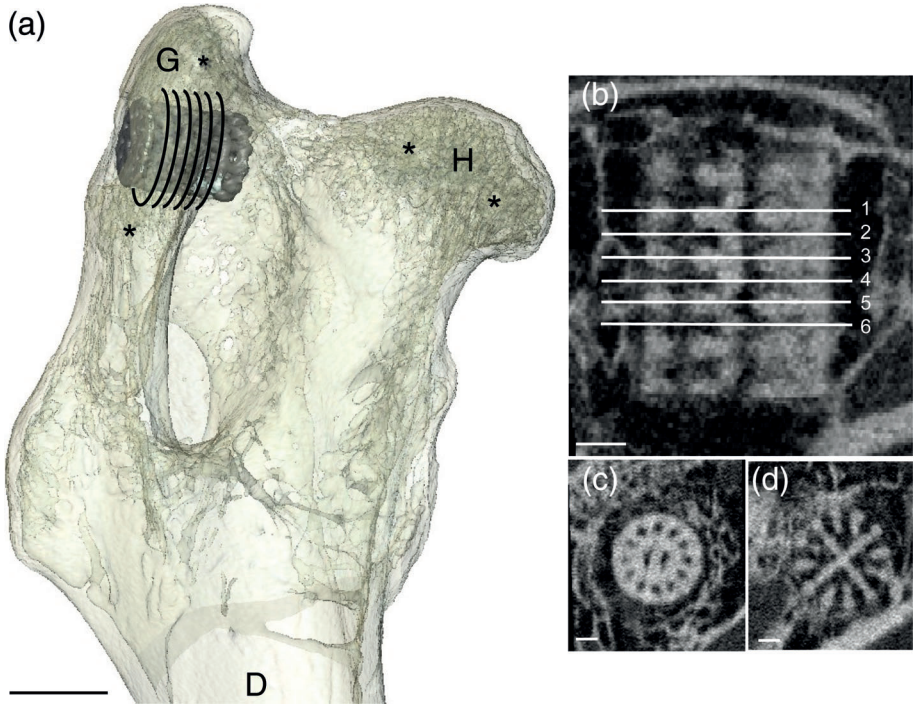

FIGURE 2 (a) Scaffold position after implantation in a rabbit femur; D, medullary canal; G, greater trochanter; H, femur head; asterisks, cancellous bone; scale bar: 5 mm; (b) μ-CT longitudinal section of a LAE442 p500 scaffold: starting from the drill hole side, six consecutive strut and pore cross sections were examined for bone-scaffold contacts in each scaffold sample, scale bar: 1 mm; (c) strut cross section, (d) pore cross section shown within a LAE442 p500 scaffold, scale bar: 1 mm

surgical field was aseptically prepared. Anaesthesia was maintained with isofluoran (1.5–2 vol% with simultaneous oxygen supply of 1 L/min) and analgesia was ensured with a fentanyl infusion of 10 μg/ml (Fentadon®, 50 μg/ml, CP-Pharma Handelsgesellschaft mbH, Burgdorf, Germany). The greater trochanter was accessed through ~2 cm long skin incision. Subcutaneous fat tissue and underlying musculature were prepared in order to expose the bone using a periosteal elevator. A 6 mm deep hole was drilled into the greater trochanter using a surgical power tool (Colibrii II, Synthes GmbH, Oberdorf, Switzerland) with a Ø 4 mm drill bit. The resulting drilling residues were eliminated by suction. The scaffold was placed approximately 1 mm below the outer contour of the bone (Figure 2a). The wound was then sutured in layers with absorbable sutures (Monosyn® 4/0, B. Braun Surgical S.A., Rubi, Spain) and the overlying skin was closed with non-absorbable sutures (Optilene® 4/0, B. Braun Surgical S.A.). Postoperatively, each animal received a single intravenous dose of 20 μg/kg buprenorphine (Bupresol®, 0.3 mg/ml, CP-Pharma Handelsgesellschaft mbH, Burgdorf, Germany). From the time of surgery up to the fifth day postoperative, 10 mg/kg/day enrofloxacin (Enrobactin®, 25 mg/ml, CP-Pharma Handelsgesellschaft mbH, Burgdorf, Germany) and 0.3 mg/kg/day meloxicam (Rheumocam®, 1.5 mg/ml, Boehringer Ingelheim Pharma GmbH & Co. KG, Ingelheim am Rhein, Germany) were given orally. A general examination of the animals as well as wound and lameness examinations were carried out daily.

2.4 | X-ray investigations

The pelvis and the femora were X-rayed in ventrodorsal position directly after surgery, in the further course every 2 weeks until week 12, then every 4 weeks until week 36 (Multix Secret DR, Siemens, Erlangen, Germany, 4.5 mA s, 55 kV). The evaluation was carried out with the software dicomPACS® vet (version 8.3.20; Oehm und Rehbein GmbH, Rostock, Germany). Based on a study by Lalk et al. (2010), a semiquantitative scoring system was used to determine the following parameters: gas outside the bone (descriptive), periosteal bone formation in the region of the implant site (mm), bone-like structures in the surrounding muscle tissue (number and size in mm). The scores ranged from 0 (unchanged state) to 2 (clearly altered). In addition, the visibility of the scaffolds was evaluated with the score values 0 (visible) and 1 (not visible) (Table 1).

TABLE 1 Scoring system used for evaluation of bone and scaffold related changes at the implantation site as observed on radiographs in ventrodorsal position

Parameter	Score 0	Score 1	Score 2
Gas	None	Few or diffuse	Clear and measurable bubbles
Bone-like structures in surrounding muscles	None	1–3 structures of ≤2 mm	1–3 structures >2 mm or > 3 structures
Periosteal bone formation	None	≤ 7 mm in length and ≤ 2 mm wide	>7 mm in length and >2 mm wide
Visibility of the scaffold	Yes	No	–

2.5 | In vivo μ-CT investigation

The μ-computer tomography examinations (XtremeCT II, Scanco Medical, Zurich, Switzerland) were also performed directly after surgery and subsequently at the same times as the X-ray examinations. The following settings were used: isotropic voxel size: 30.3 μm, tube voltage: 68 kV, current: 1470 μA, projections: 1000/180°, integration time: 200 ms. For the μ-CT scans the animals were given an intramuscular anaesthesia (0.15 mg/kg ketamine, Anesketin® 100 mg/ml, Albrecht GmbH, Aulendorf, Germany; 0.25 mg/kg medetomidine, Dorbene vet® 1 mg/ml, Zoetis Deutschland GmbH, Berlin, Germany). The scanning area was defined from just below the lesser trochanter to about 5 mm above the greater trochanter. The μ-CT analyses were performed in two and three dimensions.

2.5.1 | Semiquantitative in vivo 2D evaluation in scaffold longitudinal and cross section

Evaluation of gas formation and bony reactions in the scaffold longitudinal section

The evaluation of the 2D cross-sectional images was based on the established semiquantitative scoring system by Lalk et al. (2010) (Table 2). In the longitudinal sections of the scaffolds, the following parameters were evaluated: location of the scaffolds, gas formation in the bone in three different locations (within the scaffold/around the scaffold/in the medullary canal), periosteal bone formation (length in mm), bone-like structures in the surrounding musculature (number and size in mm) and drill hole closure. Scores for the scaffold location ranged from score 0 (completely embedded in cancellous bone) to 2 (mainly in medullary canal or penetrating through corticalis) and were evaluated in the first scan. The other score parameters ranged from 0 (unchanged state/not existing) to 2 (clearly altered). The scores of gas accumulation in the different bone locations were added up to give a total score.

Evaluation of the bone-scaffold contacts in the scaffold cross section

To obtain uniform cross-sectional views for the evaluation of the scaffolds, the scaffold longitudinal sections were manually contoured and reoriented using the μ-CT evaluation program V 6.4-2 (Scanco Medical, Zurich, Switzerland). Bone-scaffold contact was determined according to the protocols used by Lalk et al. (Lalk et al., 2010; Lalk et al., 2013) (Table 2). Six central cross sections per scaffold were evaluated, which were located in the cancellous area of the greater trochanter (Figure 2).

TABLE 2 Scoring system employed for in vivo μ-computer tomography (XtremeCT II)

Parameter	Score 0	Score 1	Score 2
Location of the scaffolds (at first scan directly postsurgery)	Completely embedded in cancellous bone	Mainly in cancellous bone	Mainly in medullary canal or penetrating through corticalis
Gas*			
-Within scaffold -Around scaffold -In medullary canal	None	Few or diffuse	Clear and measurable bubbles
Bone-like structures in surrounding muscles	None	1–3 structures of ≤2 mm	1–3 structures >2 mm or >3 structures
Periosteal bone formation	None	≤ 7 mm in length and ≤2 mm wide	>7 mm in length and > 2 mm wide
Drill hole closure	Closed	Partially closed	Open
Bone-scaffold contact	Many direct contact points to trabecular bone, only isolated gaps in between	Trabecular bone in surrounding but only few contacts points, clear gaps in between	No contact to trabecular bone, complete gap around the scaffold

Note: Parameters were evaluated over the entire scan area, while the bone-scaffold contact was evaluated in six cross sections through the scaffolds (starting from the drill hole direction: 3× pore-section, 3× strut-section alternately), cross sections shown in Figure 2(c) and (d). The individual gas values (*) were summed up to a total score.

2.5.2 | Quantitative in vivo 3D evaluation

For the quantitative 3D evaluation, it was necessary to determine the respective threshold for LAE442 (146), ß-TCP (148), and for cancellous bone (120). Five femora of healthy rabbits of the same breed and age were scanned without scaffolds to determine the threshold of cancellous bone in the greater trochanter. Two "regions of interest" (ROI) were defined for the evaluation of scaffold degradation and osseointegration in vivo.

Evaluation of scaffold degradation

The first ROI was determined by placing a standardized cylinder in the middle part of the scaffold with a diameter of 132 voxels (equivalent to 3.99 mm). The height of the cylinder was 50 slices (equivalent to 1.52 mm) for p400 and 60 slices for p500 and ß-TCP (equivalent to 1.82 mm) (Xu et al., 2018). The different heights resulted from the two different pore sizes of the LAE442 scaffolds and were chosen for both types of the scaffolds so that the same two pore and strut sections were always included in the calculations (Figure 3a,b). The scaffold density (mg HA/cm^3) and the scaffold volume (mm^3) were determined each time. To compare the scaffold volumes despite the differing pore sizes, the percentage scaffold volume share (%) was additionally calculated. To calculate the in vivo corrosion rate, the scaffold volume (mm^3) and the scaffold surface (mm^2) were determined.

Evaluation of osseointegration in the scaffold surroundings

The second ROI, a double ring around the first ROI, was set to analyse bone growth behavior (Bissinger et al., 2017). For all scaffold groups, the inner circle of the double ring had a diameter of 134 voxels (corresponding to 4.06 mm) and a distance of 400 μm to the outer circle with 159 voxels (corresponding to 4.82 mm) (Figure 3c). Within the second ROI, bone density (mg HA/cm^3), bone volume fraction (%), trabecular number (1/mm), trabecular thickness (mm), and trabecular separation (mm) were determined.

2.5.3 | In vivo corrosion rate of the scaffolds

The determined μ-CT data sets were used to calculate the in vivo corrosion rates of the scaffolds as a function of volume loss and implant duration using $CR = \Delta V/(A \times t)$ (Witte et al., 2006). CR represents the in vivo corrosion rate (mm/year), ΔV is the difference between the initial volume and the residual volume, A is the scaffold surface (mm^2) of the implant and t is the exposure time in days.

2.6 | Statistics

The mean values and their standard deviations were calculated from the data. The statistical evaluation was carried out with Microsoft Office Excel® Version 2016 (Microsoft Office XP, Microsoft Corporation, Redmond) and SPSS® Version 25.0 (SPSS, IBM Company, Chicago). Distribution characteristics were determined by using the Shapiro–Wilk test and histograms. Since the data did not show normal distribution, the groups were tested for significance by using the nonparametric Kruskal-Wallis test with a one-way analysis of variance (ANOVA) and subsequent Bonferroni post hoc comparison. Statistically significant differences were defined as $p < .05$.

3 | RESULTS

3.1 | Clinical examinations

Overall, none of the animals exhibited clinical adverse reactions. According to a physiological healing process, mild swelling and slight redness occurred around the surgical site. These disappeared in all cases within the first days after surgery and did not lead to any impairment of the animals. There was no evidence of infection of the bone or soft tissue. Lameness and signs of pain could not be detected

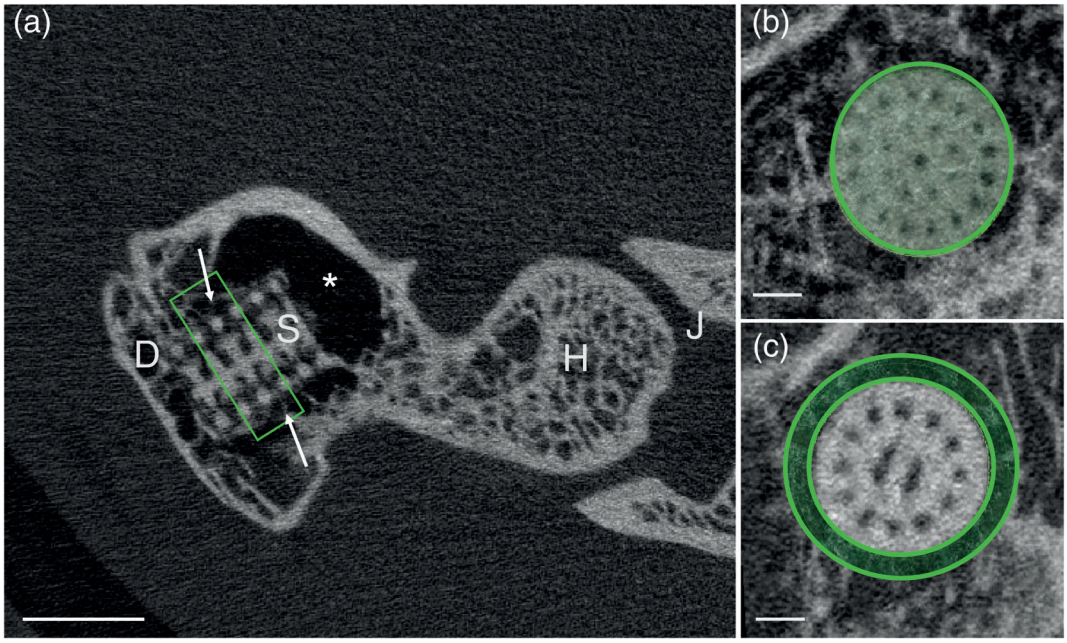

FIGURE 3 (a) Longitudinal section of scaffold, green box, area of quantitative 3D measurements; D, periosteal bone formation; H, femur head; J, hip joint and acetabulum; S, scaffold; arrows, trabecular meshwork with scaffold contacts; asterisk, medullary cavity; (b) first ROI for scaffold degradation; (c) second ROI within a 400 μm wide double ring around the scaffold where bone values were measured

in any animal. Emphysematous swellings were not present over the whole investigation period.

3.2 | Radiological evaluation

There was no gas accumulation in the surrounding soft tissue for p400 and ß-TCP at any time except immediately after surgery. In the p500 scaffold group, two animals showed a mild gas accumulation in the soft tissue close to the implant site up to week 4 and week 6, respectively. All scaffolds of p400 and p500 were clearly visible over the entire 36-week period. Single ß-TCPs were no longer recognizable from week 10 and were no longer visible at all from week 24 onwards.

Postoperatively, periosteal bone formation was found in the area of the implant site, which steadily increased in size over time and reached an average length of >7 mm in all scaffold groups up to week 36. In addition, smaller bone-dense structures were found in the muscle tissue near the implant site, which increased in size over time.

3.3 | Semiquantitative in vivo μ-CT evaluations

3.3.1 | Results of gas formation and bone reactions in the 2D scaffold longitudinal section

All scaffolds were precisely inserted into the intended cancellous part of the greater trochanter (Figure 4a). Gas formation was observed for p400 and p500 over the entire duration of the study. The highest increase in gas was noted directly postoperative up to week 2. At that time, p400 showed significantly more gas than p500 (p = .047). In comparison, the presence of gas was only noted directly postoperative in the ß-TCP group. Overall, p500 showed less gas accumulation than p400. The two LAE442 scaffolds increased their gas formation until week 20 and subsequently decreased to a moderate amount in week 36 (Figure 4b).

Small periosteal bone formations around the implant site were already detected in week 2 in all scaffolds. These increased in size and reached maximum values of 19.1 mm × 3.3 mm in the p400 group (week 28), 19.4 mm × 2.7 mm in the p500 group (week 24) and 23.6 mm × 5.9 mm in the ß-TCP group (week 16). Small, bone-like structures were also found in the surrounding muscle tissue, which became larger over time (Figure 4c,d).

The fastest drill hole closure was detected with the ß-TCP scaffolds (Figure 4e). In week 6 85% of the 40 ß-TCPs showed a compact, bony layer above the drill site. In p400 63.3% of the scaffolds showed a drill hole closure at week 12, and in p500 76.6% of the drill holes were closed at week 12. One drill hole in both p400 and p500 scaffold groups stayed incompletely covered with bone until the end of the 36-week investigation period.

3.3.2 | Bone-scaffold contact in 2D scaffold cross sections

In the initial stage, the two pore sizes of the LAE442 scaffolds showed only isolated bone-scaffold contacts. After week 12 (p400) and 16 (p500) the number of detected contacts increased until week 36. Although p500 always showed more bone-scaffold contacts than

p400 based on the scores, differences between both pore sizes were significant only in week 2 (p = .007). In comparison, ß-TCP already showed numerous bone-scaffold contacts in week 2, which increased in number by week 36. ß-TCP showed therefore significant differences to p400 and p500 at any time (p = <.05) (Figures 4f and 5).

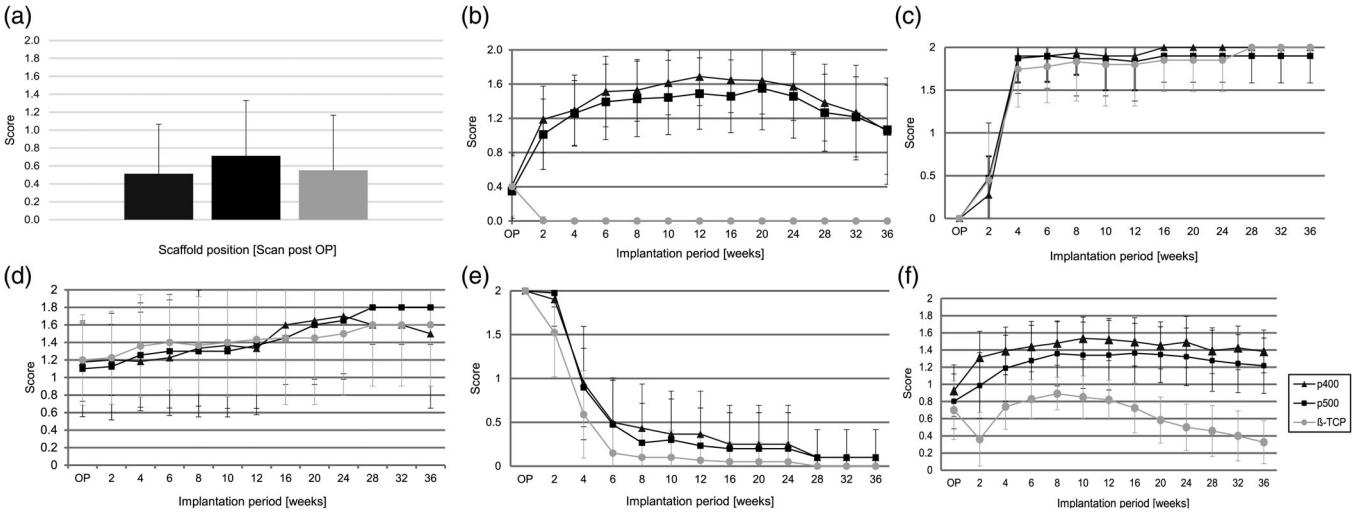

FIGURE 4 2D semiquantitative evaluation of the in vivo μ-CT parameters (a) location of the scaffolds; (b) gas accumulation; (c) periosteal bone formation; (d) bone-like structures in the surrounding musculature; (e) drill hole closure; (f) bone-scaffold contact. (a)–(e) were evaluated using the longitudinal view of scaffolds, (f) was evaluated using the cross-sectional view of scaffolds

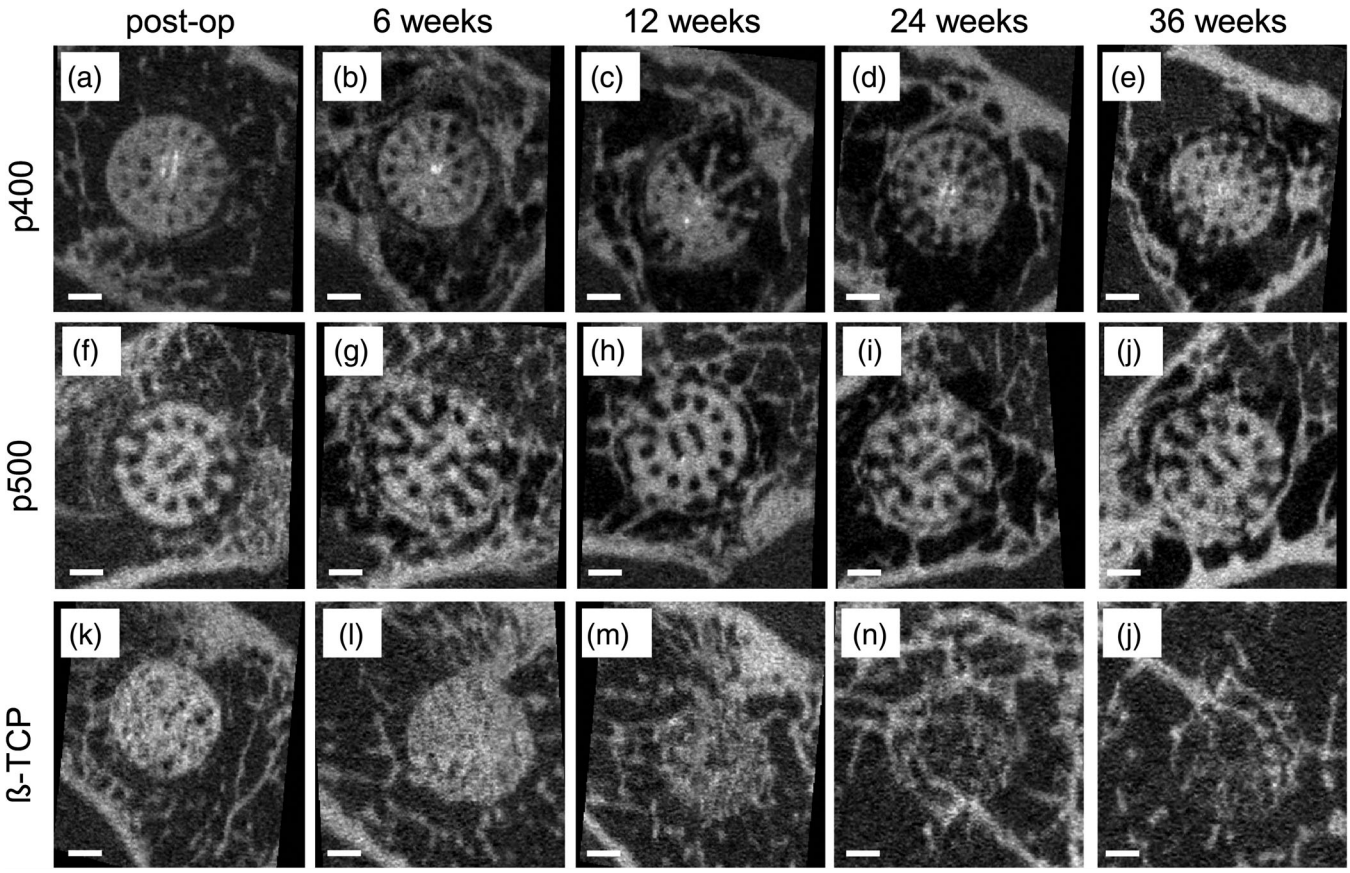

FIGURE 5 Osseointegration behavior based on reoriented scaffold cross sections: one sample per scaffold group over the study period post op, 6, 12, 24, and 36 weeks with increasing number of bone-scaffold contacts. (b)–(e) and (g)–(j): gas accumulation (black areas around both types of the LAE442 scaffolds)

3.4 | Quantitative in vivo 3D evaluation

3.4.1 | Results of scaffold degradation

The density of LAE442 scaffolds decreased only slightly with 2% for p400 and 1.8% for p500 after week 36, respectively, regardless of pore size, whereas ß-TCP showed a density loss of 6.4% after week 36 (Figure 6a). The calculated scaffold volume decreased by a total of 15.9% for p400 and 11.1% for p500 by week 36. The largest volume loss occurred between the time directly postoperative and week 2 for p400 with 7.5% and p500 with 6%. In contrast, the volume of ß-TCP was reduced by more than half after week 12 and dropped to 25.4% of the original volume by week 36 (Figure 6b).

Both LAE442 scaffolds showed the fastest in vivo corrosion rate between directly postoperative and week 2, with 3.76×10^{-1} mm/year for p400 and 2.86×10^{-1} mm/year for p500. Subsequently both slowed down to an average rate of 4.55×10^{-2} mm/year for p400 and 3.71×10^{-2} mm/year for p500 after 36 weeks. ß-TCP degraded fastest from week 4 to week 6 with 2.09 mm/year and had significantly higher in vivo corrosion rates than the LAE442 scaffolds at any time.

3.4.2 | Results of bone remodeling in the scaffold surroundings

Bone density increased in both pore sizes after surgery and exceeded the comparison values of cancellous rabbit bones (733.3 mg HA/cm^3) at weeks 16 (p400) and 24 (p500). ß-TCP also showed an overall increase in bone density in the immediate vicinity of the scaffolds, which exceeded the comparison values of cancellous bone in the greater trochanter at week 6 and remained highest of all material groups (Figure 7a). The bone volume fraction in the scaffold environment was similar for all three scaffold groups. After an initial increase, the volumes leveled to values in the cancellous bone area from week 8. In week 2, a significantly higher bone volume was determined for p500 compared to p400 (p = .026). Later, p400 also showed the lowest bone volume fraction compared to p500 and ß-TCP (Figure 7b).

In accordance with the bone volume, the number of trabeculae for p500 and ß-TCP also increased at the beginning. From week 8 onwards, the number of trabeculae corresponded to the comparison values of cancellous bone. From week 16, p500 had a slightly higher number of trabeculae than ß-TCP. The smaller pore size p400, on the other hand, had a significantly lower trabecular number in week 2 than p500 and ß-TCP ($p \leq .007$) and was also behind in later measurements (Figure 8a).

The trabecular thickness of the LAE442 scaffolds was slightly less pronounced than that with ß-TCP. However, from week 28 onwards, p500 again reached values corresponding to the cancellous bone of nonoperated, healthy rabbits, whereas p400 showed no improvement in trabecular thickness at later points in time. The measured distances between individual trabeculae increased over time for all scaffold groups. The largest trabecular separation was always determined for p400, followed by p500 and finally ß-TCP (Figure 8a,b).

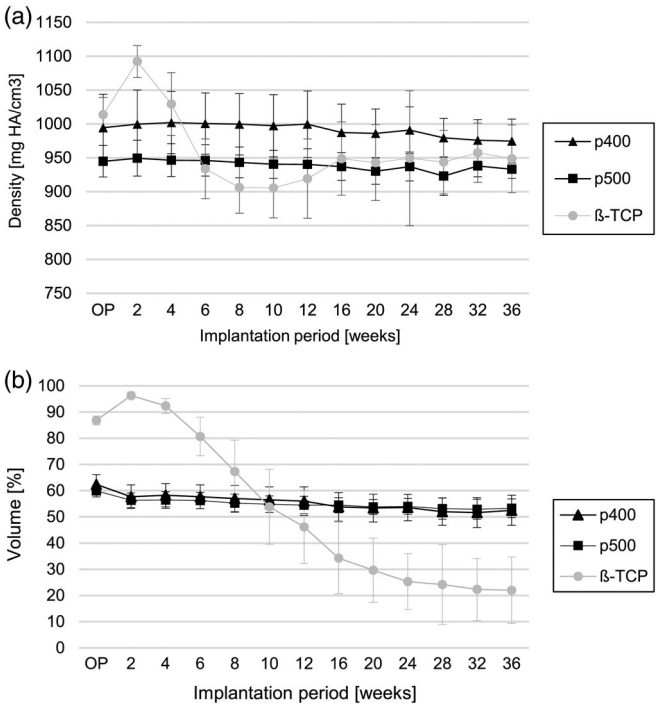

FIGURE 6 3D quantitative evaluation of the in vivo µ-CT: (a) scaffold density (mg HA/cm^3) and (b) percentage scaffold volume share (%) were calculated over a study duration up to 36 weeks (ROI for measuring the scaffold degradation)

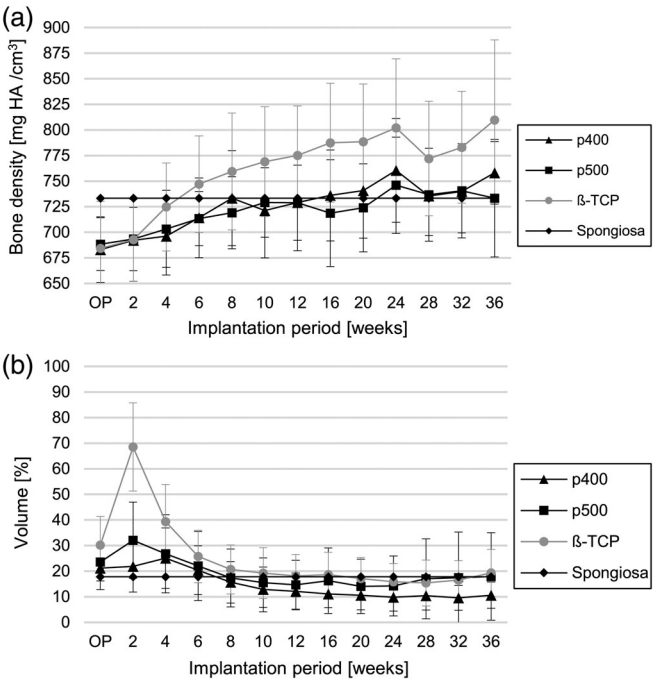

FIGURE 7 3D quantitative evaluation of the in vivo µ-CT: (a) bone density (mg HA/cm^3) and (b) bone volume (%) were measured during the implantation period up to 36 weeks in the ROI within a 400 µm wide double ring around the scaffolds

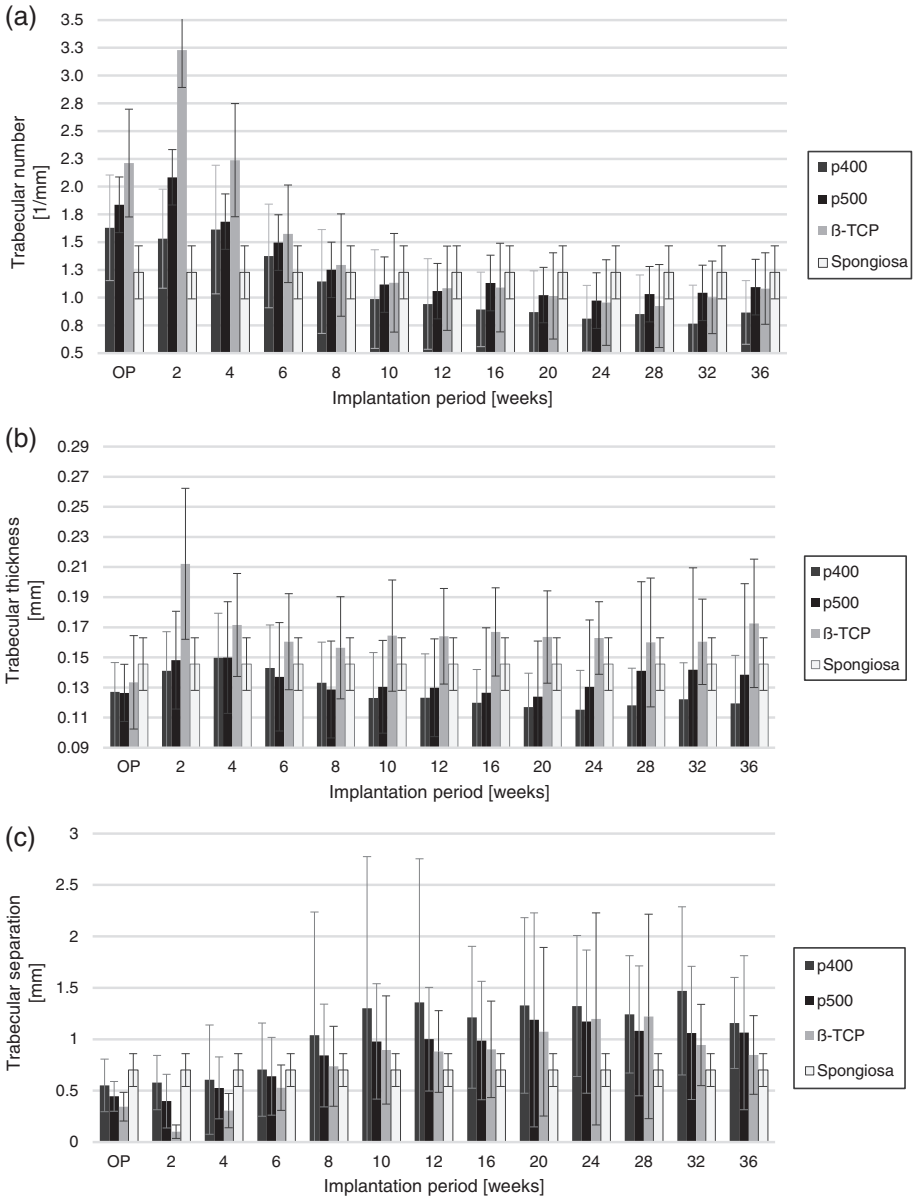

FIGURE 8 3D quantitative evaluation of trabecular values from in vivo µ-CT during the implantation period: (a) trabecular number (1/mm), (b) trabecular thickness (mm), and (c) trabecular separation (mm) for an ROI within a 400 µm wide double ring around the scaffolds

4 | DISCUSSION

The LAE442 alloy has already been classified by in vivo studies as a biocompatible and slowly degrading bone substitute (Angrisani et al., 2012; Angrisani et al., 2016; Hampp et al., 2013; Meyer-Lindenberg et al., 2010; Reifenrath et al., 2010; Rossig et al., 2015; Thomann et al., 2009; Witte et al., 2005; Witte et al., 2006). So far, however, only solid implants from LAE442 have been investigated (Angrisani et al., 2016; Hampp et al., 2013; Krause et al., 2009; Meyer-Lindenberg et al., 2010; Reifenrath et al., 2010; Rossig et al., 2015; Thomann et al., 2009; Witte et al., 2005; Witte et al., 2006; Witte et al., 2010; Wolters et al., 2013). LAE442 was investigated in this study for the first time as an open-pored scaffold with a reproducible arrangement of defined pores in rabbit femur. It is known that bone substitute materials with pores as a structural factor favor the ingrowth of blood vessels and cell migration and thus promote osteogenesis (Karageorgiou & Kaplan, 2005; Klenke et al., 2008). Lalk et al. (2013) already investigated the Mg alloy AX30 with inhomogeneous pore distribution and size in preliminary studies in rabbits. Despite good osseointegration, the cylindrical Mg sponge structures degraded too quickly. For the current study, scaffolds of the Mg alloy LAE442 with uniform defined pore sizes and the ceramic ß-TCP as control group were investigated in the cancellous part of the greater trochanter of rabbits. The animals were examined clinically and with imaging techniques (RX, µ-CT) over a period up to 36 weeks and the implanted scaffolds were analyzed for their degradation and osseointegration behavior.

The implantation-related surgical wounds healed without any clinical complications. Subcutaneous emphysema, which occurred in previous studies in LAE442 near the implant site (Hampp et al., 2013; Witte et al., 2005; Wolters et al., 2013), was not observed in the present study. Accordingly, LAE442 scaffolds p400 and p500 were

tolerated clinically as well as ß-TCP. No animal showed lameness or signs of pain. These results are consistent with previous in vivo studies, which also investigated the degradation behavior of LAE442 over longer time periods (Angrisani et al., 2016; Meyer-Lindenberg et al., 2010; Rossig et al., 2015).

Periosteal bone formation and smaller bone-like structures in the surrounding soft tissue close to the implant site were visible in x-ray and in vivo μ-CT of all three scaffold groups. These observations were also described by Lalk et al. (2013) who examined AX30 sponge structures at the same implant site in rabbits. Other authors also reported bone formation at the site of insertion of LAE442 implants placed in the tibia (Hampp et al., 2013; Rossig et al., 2015; Thomann et al., 2009). The stimulating effect of magnesium on bone growth (Revell, Damien, Zhang, Evans, & Howlett, 2004; Zreiqat et al., 2002) is discussed here, but the surgical procedure, especially the drilling process, may also have an influence on the development of periosteal growth (Danckwardt-Lilliestrom, 1969; Höh et al., 2009).

The implanted LAE442 scaffolds p400 and p500 were clearly visible on X-rays throughout the study. This observation matches the μ-CT results with only minimal decrease in density and small volume losses. The small standard deviations of the volume losses that occurred at the individual points in time could indicate a homogeneous degradation of the LAE442 scaffolds (Huehnerschulte et al., 2012). Angrisani et al. (Angrisani et al., 2016) recorded a volume loss of 2% of intramedullary LAE442 pins after 36 weeks for cylindrical implants without pores, whereas the LAE442 scaffolds used in this study degraded faster. Reasons for this deviation could be the varying implantation site (Wolters et al., 2013) with associated different blood perfusion (Kraus et al., 2018) and the porosity of the LAE442 scaffolds enlarging the contact surface (Karageorgiou & Kaplan, 2005). Compared to the aforementioned porous Mg sponges of the alloy AX30, which showed a volume loss of about 76% after 24 weeks (Lalk et al., 2013), LAE442 with homogeneous pore structure degraded to a lesser extent (μ-CT: 15.9% for p400 and 11.1% after 36 weeks). In the present study, p400 showed a somewhat stronger percentage of volume loss compared to p500. This difference may be due to deviating scaffold geometries (Wolters et al., 2013). P400 includes thinner strut elements with a rougher surface and a slightly higher porosity (Julmi et al., 2019), this may lead to a higher contact surface with the host tissue, being more susceptible to degradation (Karageorgiou & Kaplan, 2005).

In comparison with the LAE442 scaffolds, the tendency of an irregular degradation of ß-TCP over time could be observed in the X-ray evaluations as well as in the μ-CT scans. A decrease in volume of 74.6% (μ-CT) by the end of the observation period, together with larger standard deviations, indicate a more irregular degradation of ß-TCP (Huehnerschulte et al., 2012; Nuss & von Rechenberg, 2008). This inhomogeneous degradation behavior paired with the brittle properties of ß-TCP limits its use as a bone substitute in weight-bearing bone (Nuss & von Rechenberg, 2008).

The results obtained for the in vivo corrosion rate showed that the LAE442 scaffolds degraded significantly slower than ß-TCP. In both LAE442 scaffolds, the fastest corrosion rate and the largest volume loss occurred between direct postoperative and week 2. This matches the tendency of an initially accelerated degradation of LAE442 that was observed in other studies in rabbits (Krause et al., 2009; Ullmann, Reifenrath, Seitz, Bormann, & Meyer-Lindenberg, 2013) and guinea pigs (Witte et al., 2005; Witte et al., 2006). It is assumed that this can be attributed to the drop in pH value after implantation of the Mg implants, which favors Mg degradation. As a possible reason for the subsequent reduction of degradation, it is described that a protective layer of calcium and phosphorus forms around the scaffolds at later experimental points (Witte et al., 2005). This phenomenon could explain the slowdown in the in vivo corrosion rates of LAE442 after week 2.

Bone-scaffold contact sites were observed in all three scaffold groups. However, there were differences in the amount of these contacts. Compared to p400, p500 showed a higher number of bone-scaffold contacts with significantly more contacts at week 2. P500 also showed a higher bone volume fraction and a higher number of trabeculae in the scaffold environment than p400 in the quantitative 3D analyses over the entire period. These two parameters differed significantly at week 2 after surgery. Similar results were also observed in the study by Cheng et al. (2016). In that study, pure Mg scaffolds with pore sizes of 250 and 400 μm were investigated in rabbit femora for their influence on bone formation. After 16 weeks, more bone tissue was present around the Mg scaffolds with the larger pore size. Lalk et al. (2013) also described a better osseointegration of porous, coated AX30 scaffolds with a pore size of about 400 μm compared to scaffolds with a smaller pore size of about 100 μm. Controversially, other studies showed no differences between different pore sizes on bone ingrowth behavior (Ayers et al., 1999; Fisher et al., 2002; Kujala, Ryhänen, Danilov, & Tuukkanen, 2003). However, other materials such as nickel, titanium, or polymers were used, so these results may not be necessarily comparable to the ones obtained for the LAE442 alloy.

The bone-scaffold contacts of p400 and p500 were observed to be thin and finely woven. Fine woven bone contacts have also been described in studies on solid intramedullary LAE442 pins in rabbit models (Angrisani et al., 2016; Hampp et al., 2013; Thomann et al., 2009). Compared to LAE442, the bone-scaffold contacts of ß-TCP in the present study were already well defined after 2 weeks and there were significant differences compared to p400 and p500 until the end of the study. ß-TCP had a higher bone volume, a larger number of trabeculae and greater trabecular thickness than p400. Later, p500 showed similar bone volume and trabecular number in the scaffold environment compared to ß-TCP. This indicates that the larger pore size p500 had better osteoconductive properties than p400 in the current study. It should be noted that the comparison between the control group and LAE442 scaffolds might be hampered by the fact of varying pore structure. The biocompatible ß-TCP ceramic (Nuss & von Rechenberg, 2008; von Doernberg et al., 2006) was selected as a control, however, it was not possible to manufacture the implants with the same geometry as the porous LAE442.

The LAE442 scaffolds showed gas accumulations in the surroundings of the implant during the weeks after surgery. A slightly more

pronounced gas development was found for p400 than for p500. This observation could be related to the higher degradation of p400, since it has already been described in the literature that a faster degradation of Mg alloys produces more gas (Song & Atrens, 1999; Staiger et al., 2006). However, as in other studies, the gas did not lead to any clinical side effects (Angrisani et al., 2016; Rossig et al., 2015). In the present study, an increase in trabecular thickness and bone volume in the scaffold environment of LAE442 was observed parallel with the decrease in gas volumes from week 20 onwards. In an investigation of ZX50 pins in a rat model, Kraus et al. (Kraus et al., 2012) also observed that bone augmentation could take place after gas reduction. It is therefore important that gas formation and absorption remain in tolerable limits for the body so that the bone formation and remodeling is not impaired.

Basically, the pore size p500 showed slower in vivo degradation than p400. With overall higher bone formation and initially reduced gas production, this leads to a more promising osseointegration of LAE442 p500 at early stages of the bone remodeling process. Later in time there were no further significant differences for the two pore sizes. However, LAE442 p400 remained slightly below the level of p500 overall in the analyses.

5 | CONCLUSION

The pore sizes p400 and p500 of the Mg alloy LAE442 showed the same good clinical tolerability as the control group ß-TCP, due to the absence of negative clinical side effects over an investigation period up to 36 weeks. The homogeneous degradation behavior of the open-pored LAE442 scaffolds resulted in an only slight volume reduction at the end of the study. The osseointegration behavior was more pronounced in p500 than in p400. Thus, LAE442 scaffolds appear attractive for use as potential bone substitutes for clinical interventions on weight-bearing bone. The prerequisite for a later clinical application of LAE442 as a bone substitute is a more controlled gas production by accordingly optimizing alloy compositions and surface coatings, and further improvement of bone ingrowth behavior.

ACKNOWLEDGMENTS

The authors thank the German Research Foundation for its financial support within the project “Interfacial effects and integration behaviour of magnesium-based sponges as bioresorbable bone substitute material” (Grant No. 271761343). Furthermore, the authors thank Lisa Wurm and Beatrix Limmer for their outstanding technical assistance.

CONFLICT OF INTEREST

The authors hereby declare that none of them has any conflict of interest with the content of the article.

REFERENCES

Agarwal, S., Curtin, J., Duffy, B., & Jaiswal, S. (2016). Biodegradable magnesium alloys for orthopaedic applications: A review on corrosion, biocompatibility and surface modifications. *Materials Science & Engineering. C, Materials for Biological Applications*, *68*, 948–963.

Angrisani, N., Reifenrath, J., Zimmermann, F., Eifler, R., Meyer-Lindenberg, A., Vano-Herrera, K., & Vogt, C. (2016). Biocompatibility and degradation of LAE442-based magnesium alloys after implantation of up to 3.5years in a rabbit model. *Acta Biomaterialia*, *44*, 355–365.

Angrisani, N., Seitz, J.-M., Meyer-Lindenberg, A., & Reifenrath, J. (2012). Rare earth metals as alloying components in magnesium implants for orthopaedic applications. In *New Features on Magnesium Alloys*. Rijeka, Croatia: Intech.

Arrington, E. D., Smith, W. J., Chambers, H. G., Bucknell, A. L., & Davino, N. A. (1996). Complications of iliac crest bone graft harvesting. *Clinical Orthopaedics and Related Research*, *329*, 300–309.

Ayers, R. A., Simske, S. J., Bateman, T. A., Petkus, A., Sachdeva, R. L. C., & Gyunter, V. E. (1999). Effect of nitinol implant porosity on cranial bone ingrowth and apposition after 6 weeks. *Journal of Biomedical Materials Research*, *45*(1), 42–47.

Banwart, J. C., Asher, M. A., & Hassanein, R. S. (1995). Iliac crest bone graft harvest donor site morbidity. *A Statistical Evaluation. Spine (Phila pa 1976)*, *20*(9), 1055–1060.

Bergsma, E. J., Rozema, F. R., Bos, R. R. M., & Bruijn, W. C. D. (1993). Foreign body reactions to resorbable poly(l-lactide) bone plates and screws used for the fixation of unstable zygomatic fractures. *Journal of Oral and Maxillofacial Surgery*, *51*(6), 666–670.

Bissinger, O., Probst, F. A., Wolff, K.-D., Jeschke, A., Weitz, J., Deppe, H., & Kolk, A. (2017). Comparative 3D micro-CT and 2D histomorphometry analysis of dental implant osseointegration in the maxilla of minipigs. *Journal of Clinical Periodontology*, *44*(4), 418–427.

Bobyn, J. D., Pilliar, R. M., Cameron, H. U., & Weatherly, G. C. (1980). The optimum pore size for the fixation of porous-surfaced metal implants by the ingrowth of bone. *Clinical Orthopaedics and Related Research*, *150*, 263–270.

Bohner, M., Baroud, G., Bernstein, A., Döbelin, N., Galea, L., Hesse, B., Heuberger, R., Meille, S., Michel, P., von Rechenberg, B., Sague, J., & Seeherman, H. (2017). Characterization and distribution of mechanically competent mineralized tissue in micropores of β-tricalcium phosphate bone substitutes. *Materials Today*, *20*(3), 106–115.

Böstman, O., Hirvensalo, E., Vainionpää, S., Mäkelä, A., Vihtonen, K., Törmälä, P., & Rokkanen, P. (1989). Ankle fractures treated using biodegradable internal fixation. *Clinical Orthopaedics and Related Research*, *238*, 195–203.

Cheng, M. Q., Wahafu, T., Jiang, G. F., Liu, W., Qiao, Y. Q., Peng, X. C., Cheng, T., Zhang, X. L., He, G., & Liu, X. Y. (2016). A novel open-porous magnesium scaffold with controllable microstructures and properties for bone regeneration. *Scientific Reports*, *6*, 24134.

Danckwardt-Lilliestrom, G. (1969). Reaming of the medullary cavity and its effect on diaphyseal bone: A fluorochromic, microangiographic and histologic study on the rabbit tibia and dog femur. *Acta Orthopaedica Scandinavica*, *40*(sup128), 1–165.

Fisher, J. P., Vehof, J. W., Dean, D., van der Waerden, J. P. C., Holland, T. A., Mikos, A. G., & Jansen, J. A. (2002). Soft and hard tissue response to photocrosslinked poly (propylene fumarate) scaffolds in a rabbit model. *Journal of Biomedical Materials Research*, *59*(3), 547–556.

Galois, L., & Mainard, D. (2004). Bone ingrowth into two porous ceramics with different pore sizes: An experimental study. *Acta Orthopaedica Belgica*, *70*(6), 598–603.

Hampp, C., Angrisani, N., Reifenrath, J., Bormann, D., Seitz, J. M., & Meyer-Lindenberg, A. (2013). Evaluation of the biocompatibility of two magnesium alloys as degradable implant materials in comparison to titanium as non-resorbable material in the rabbit. *Materials Science & Engineering. C, Materials for Biological Applications*, *33*(1), 317–326.

Hofmann, S., Hilbe, M., Fajardo, R. J., Hagenmuller, H., Nuss, K., Arras, M., Müller, R., von Rechenberg, B., Kaplan, D. L., Merkle, H. P., & Meinel, L. (2013). Remodeling of tissue-engineered bone structures

in vivo. *European Journal of Pharmaceutics and Biopharmaceutics*, *85*(1), 119–129.

Höh, N. V. D., Bormann, D., Lucas, A., Denkena, B., Hackenbroich, C., & Meyer-Lindenberg, A. (2009). Influence of different surface machining treatments of magnesium-based Resorbable implants on the degradation behavior in rabbits. *Advanced Engineering Materials*, *11*(5), B47–B54.

Huehnerschulte, T. A., Reifenrath, J., von Rechenberg, B., Dziuba, D., Seitz, J. M., Bormann, D., … Meyer-Lindenberg, A. (2012). In vivo assessment of the host reactions to the biodegradation of the two novel magnesium alloys ZEK100 and AX30 in an animal model. *Biomedical Engineering Online*, *11*, 14.

Hulbert, S. F., Young, F. A., Mathews, R. S., Klawitter, J. J., Talbert, C. D., & Stelling, F. H. (1970). Potential of ceramic materials as permanently implantable skeletal prostheses. *Journal of Biomedical Materials Research*, *4*(3), 433–456.

Ignatius, A. A., Augat, P., Ohnmacht, M., Pokinskyj, P., Kock, H. J., & Claes, L. E. (2001). A new bioresorbable polymer for screw augmentation in the osteosynthesis of osteoporotic cancellous bone: A biomechanical evaluation. *Journal of Biomedical Materials Research*, *58*(3), 254–260.

Itälä, A. I., Ylänen, H. O., Ekholm, C., Karlsson, K. H., & Aro, H. T. (2001). Pore diameter of more than 100 μm is not requisite for bone ingrowth in rabbits. *Journal of Biomedical Materials Research*, *58*(6), 679–683.

Julmi S, Klose C, Krüger A-K, Wriggers P, Maier HJ. Development of sponge structure and casting conditions for absorbable magnesium bone implants. TMS 2017 146th Annual Meeting & Exhibition Supplemental Proceedings; 2017. p 307–317.

Julmi, S., Krüger, A.-K., Waselau, A.-C., Meyer-Lindenberg, A., Wriggers, P., Klose, C., & Maier, H. J. (2019). Processing and coating of open-pored absorbable magnesium-based bone implants. *Materials Science and Engineering: C*, *98*, 1073–1086.

Karageorgiou, V., & Kaplan, D. (2005). Porosity of 3D biomaterial scaffolds and osteogenesis. *Biomaterials*, *26*(27), 5474–5491.

Klenke, F. M., Liu, Y., Yuan, H., Hunziker, E. B., Siebenrock, K. A., & Hofstetter, W. (2008). Impact of pore size on the vascularization and osseointegration of ceramic bone substitutes in vivo. *Journal of Biomedical Materials Research Part A*, *85A*(3), 777–786.

Kraus, T., Fischerauer, S., Treichler, S., Martinelli, E., Eichler, J., Myrissa, A., … Weinberg, A. M. (2018). The influence of biodegradable magnesium implants on the growth plate. *Acta Biomaterialia*, *66*, 109–117.

Kraus, T., Fischerauer, S. F., Hanzi, A. C., Uggowitzer, P. J., Loffler, J. F., & Weinberg, A. M. (2012). Magnesium alloys for temporary implants in osteosynthesis: in vivo studies of their degradation and interaction with bone. *Acta Biomaterialia*, *8*(3), 1230–1238.

Krause, A., von der Höh, N., Bormann, D., Krause, C., Bach, F.-W., Windhagen, H., & Meyer-Lindenberg, A. (2009). Degradation behaviour and mechanical properties of magnesium implants in rabbit tibiae. *Journal of Materials Science*, *45*(3), 624–632.

Kuboki, Y., Takita, H., Kobayashi, D., Tsuruga, E., Inoue, M., Murata, M., Nagai, N., Dohi, Y., & Ohgushi, H. (1998). BMP-induced osteogenesis on the surface of hydroxyapatite with geometrically feasible and nonfeasible structures: Topology of osteogenesis. *Journal of Biomedical Materials Research*, *39*(2), 190–199.

Kujala, S., Ryhänen, J., Danilov, A., & Tuukkanen, J. (2003). Effect of porosity on the osteointegration and bone ingrowth of a weight-bearing nickel–titanium bone graft substitute. *Biomaterials*, *24*(25), 4691–4697.

Lalk, M., Reifenrath, J., Angrisani, N., Bondarenko, A., Seitz, J.-M., Mueller, P. P., & Meyer-Lindenberg, A. (2013). Fluoride and calcium-phosphate coated sponges of the magnesium alloy AX30 as bone grafts: A comparative study in rabbits. *Journal of Materials Science: Materials in Medicine*, *24*(2), 417–436.

Lalk, M., Reifenrath, J., Rittershaus, D., Bormann, D., & Meyer-Lindenberg, A. (2010). Biocompatibility and degradation behaviour of degradable magnesium sponges coated with bioglass – Method establishment within the framework of a pilot study. *Materialwissenschaft und Werkstofftechnik*, *41*(12), 1025–1034.

Lambotte, A. (1932). L'utilisation du magnesium comme materiel perdu dans l'osteosynthèse. *Bull Mem Soc Nat Chir*, *28*, 1325–1334.

Mcbride, E. D. (1938). Magnesium screw and nail transfixion in fractures. *Southern Medical Journal*, *31*(5), 508–514.

Meyer-Lindenberg, A., Thomann, M., Krause, A., Bormann, D., von Rechenberg, B., & Windhagen, H. (2010). Untersuchungen zum Einsatz einer Magnesiumbasislegierung als neues resorbierbares Implantatmaterial für die Osteosynthese. *Kleintierpraxis*, *55*, 349–363.

Nuss, K. M. R., & von Rechenberg, B. (2008). Biocompatibility issues with modern implants in bone - a review for clinical orthopedics. *The Open Orthopaedics Journal*, *2*, 66–78.

Phemister, D. B. (1935). Bone growth and repair. *Annals of Surgery*, *102*(2), 261–285.

Prolo, D. J., & Rodrigo, J. J. (1985). Contemporary bone graft physiology and surgery. *Clinical Orthopaedics and Related Research*, *200*, 322–342.

Reifenrath, J., Krause, A., Bormann, D., von Rechenberg, B., Windhagen, H., & Meyer-Lindenberg, A. (2010). Profound differences in the in-vivo-degradation and biocompatibility of two very similar rare-earth containing Mg-alloys in a rabbit model. *Materialwissenschaft und Werkstofftechnik*, *41*(12), 1054–1061.

Revell, P. A., Damien, E., Zhang, X., Evans, P., & Howlett, C. R. (2004). The effect of magnesium ions on bone bonding to hydroxyapatite coating on titanium alloy implants. *Trans Tech Publications*, *254*, 447–450.

Rossig, C., Angrisani, N., Helmecke, P., Besdo, S., Seitz, J. M., Welke, B., Fedchenko, N., Kock, H., Reifenrath, J. (2015). In vivo evaluation of a magnesium-based degradable intramedullary nailing system in a sheep model. *Acta Biomaterialia*, *25*, 369–383.

Seitz, J.-M., Collier, K., Wulf, E., Bormann, D., Angrisani, N., Meyer-Lindenberg, A., & Bach, F.-W. (2011). The effect of different sterilization methods on the mechanical strength of magnesium based implant materials. *Advanced Engineering Materials*, *13*(12), 1146–1151.

Song, G. L., & Atrens, A. (1999). Corrosion mechanisms of magnesium alloys. *Advanced Engineering Materials*, *1*(1), 11–33.

Staiger, M. P., Pietak, A. M., Huadmai, J., & Dias, G. (2006). Magnesium and its alloys as orthopedic biomaterials: A review. *Biomaterials*, *27*(9), 1728–1734.

Suganuma, J., & Alexander, H. (1993). Biological response of intramedullary bone to poly-L-lactic acid. *Journal of Applied Biomaterials*, *4*(1), 13–27.

Thomann, M., Krause, C., Bormann, D., Von der Höh, N., Windhagen, H., & Meyer-Lindenberg, A. (2009). Comparison of the resorbable magnesium. Alloys LAE442 und MgCa0. 8 concerning their mechanical properties, their progress of degradation and the bone-implant-contact after 12 months implantation duration in a rabbit model. *Materialwissenschaft Und Werkstofftechnik: Entwicklung, Fertigung, Prüfung, Eigenschaften Und Anwendungen Technischer Werkstoffe*, *40*(1–2), 82–87.

Ullmann, B., Reifenrath, J., Seitz, J. M., Bormann, D., & Meyer-Lindenberg, A. (2013). Influence of the grain size on the in vivo degradation behaviour of the magnesium alloy LAE442. *Proceedings of the Institution of Mechanical Engineers. Part H*, *227*(3), 317–326.

Verbrugge, J. (1933). La tolérance du tissu osseux vis-à-vis du magnésium métallique. *Presse méd*, *55*, 1112–1114.

Verbrugge J. (1934). *Le Matériel métallique résorbable en chirurgie osseuse, par Jean Verbrugge*. Paris: Masson.

von Doernberg, M.-C., von Rechenberg, B., Bohner, M., Grünenfelder, S., van Lenthe, G. H., Müller, R., Gasser, B., Mathys, B., Baroud, G., & Auer, J. (2006). In vivo behavior of calcium phosphate scaffolds with four different pore sizes. *Biomaterials*, *27*(30), 5186–5198.

Witte, F., Fischer, J., Nellesen, J., Crostack, H. A., Kaese, V., Pisch, A., Beckmann, F., & Windhagen, H. (2006). In vitro and in vivo corrosion measurements of magnesium alloys. *Biomaterials*, *27*(7), 1013–1018.

Witte, F., Fischer, J., Nellesen, J., Vogt, C., Vogt, J., Donath, T., & Beckmann, F. (2010). In vivo corrosion and corrosion protection of magnesium alloy LAE442. *Acta Biomaterialia*, *6*(5), 1792–1799.

Witte, F., Kaese, V., Haferkamp, H., Switzer, E., Meyer-Lindenberg, A., Wirth, C., & Windhagen, H. (2005). In vivo corrosion of four magnesium alloys and the associated bone response. *Biomaterials*, *26*(17), 3557–3563.

Wolters, L., Angrisani, N., Seitz, J., Helmecke, P., Weizbauer, A., & Reifenrath, J. (2013). Applicability of degradable magnesium LAE442 alloy plate-screw-Systems in a Rabbit Model. *Biomedizinische Technik. Biomedical Engineering*, *58*(Suppl 1).

Xu, Y., Meng, H., Yin, H., Sun, Z., Peng, J., Xu, X., Guo, Q., Xu, W., Yu, X., & Yuan, Z. (2018). Quantifying the degradation of degradable implants and bone formation in the femoral condyle using micro-CT 3D reconstruction. *Experimental and Therapeutic Medicine*, *15*(1), 93–102.

Yoshikawa, H., & Myoui, A. (2005). Bone tissue engineering with porous hydroxyapatite ceramics. *Journal of Artificial Organs*, *8*(3), 131–136.

Younger, E. M., & Chapman, M. W. (1989). Morbidity at bone graft donor sites. *Journal of Orthopaedic Trauma*, *3*(3), 192–195.

Zreiqat, H., Howlett, C., Zannettino, A., Evans, P., Schulze-Tanzil, G., Knabe, C., & Shakibaei, M. (2002). Mechanisms of magnesium-stimulated adhesion of osteoblastic cells to commonly used orthopaedic implants. *Journal of Biomedical Materials Research*, *62*(2), 175–184.

How to cite this article: Augustin J, Feichtner F, Waselau A-C, et al. Comparison of two pore sizes of LAE442 scaffolds and their effect on degradation and osseointegration behavior in the rabbit model. *J Biomed Mater Res*. 2020;108B:2776–2788. https://doi.org/10.1002/jbm.b.34607